PHOTONICS Research

Liquid modified photonic crystal fiber for simultaneous temperature and strain measurement

Chupao Lin,[1,†] Ying Wang,[1,†] Yijian Huang,[1] Changrui Liao,[1,*] Zhiyong Bai,[1] Maoxiang Hou,[1] Zhengyong Li,[1] and Yiping Wang[1,2]

[1]Key Laboratory of Optoelectronic Devices and Systems of Ministry of Education and Guangdong Province, College of Optoelectronic Engineering, Shenzhen University, Shenzhen 518060, China
[2]e-mail: ypwang@szu.edu.cn
*Corresponding author: cliao@szu.edu.cn

Received 9 December 2016; revised 4 February 2017; accepted 4 February 2017; posted 13 February 2017 (Doc. ID 282595); published 6 March 2017

A liquid modified photonic crystal fiber (PCF) integrated with an embedded directional coupler and multi-mode interferometer is fabricated by infiltrating three adjacent air holes of the innermost layer with standard 1.48 refractive index liquids. The refractive index of the filled liquid is higher than that of background silica, which can not only support the transmitting rod modes but also the "liquid modified core" modes propagating between the PCF core and the liquid rods. Hence, the light propagating in the liquid modified core can be efficiently coupled into the satellite waveguides under the phase-matching conditions, resulting in a dramatic decrease of the resonant wavelength intensity. Furthermore, there is a multi-mode interference produced by modified core modes and rod modes. Such a compact (~0.91 cm) device integrated with an embedded coupler and interferometer is demonstrated for high-sensitivity simultaneous temperature (~14.72 nm/°C) and strain (~13.01 pm/$\mu\varepsilon$) measurement.

OCIS codes: (230.3990) Micro-optical devices; (060.2370) Fiber optics sensors; (060.5295) Photonic crystal fibers.

https://doi.org/10.1364/PRJ.5.000129

1. INTRODUCTION

Photonic crystal fiber (PCF) has a solid core surrounded by periodical layers of micro air holes in the cladding which exhibit many interesting properties and support a wide range of applications. One of the attractive features of this design is the light interaction it allows between the core and air hole(s) infiltrated with refractive index (RI) liquid. The infiltrated air hole then becomes an elegant sensing element for highly sensitive RI [1], temperature [2], and axial strain [2,3] measurement. Various types of liquid-filled PCF devices have been developed, including a directional coupler [4–8] and fiber in-line Mach–Zehnder interferometer [9].

Devices based on PCF with selective infiltration exhibit ultra-high sensitivity for temperature and strain measurement. However, the inherent cross-sensitivity of these kinds of devices limits their application in many areas as it introduces an unexpected measuring error. Recently, much attention has been focused on dual-parameter measurement due to its ability to resolve cross-sensitivity between different parameters. Dual-parameter sensors usually consist of two elements that possess different characteristics in the same ambient conditions; this could be achieved by cascading several fiber elements [10,11]. There are many configurations for dual-parameter sensors, including hybrid long period fiber grating (LPFG)/micro extrinsic Fabry–Perot interferometer (MEFPI) [12], highly integrated Fabry–Perot (FP)/fiber Bragg grating (FBG) [13], type II FBG/FP interferometer (FPI) [14], and multi-mode interferometer [15–17]. However, sensors cascaded with two elements inevitably enlarge the device size, and the multimode interferometers are limited by their low sensitivity.

In this paper, a liquid modified PCF is demonstrated for simultaneous temperature and strain measurement. This fiber is based on both the mode-directional coupling from the "liquid modified core" mode to the rod mode and the multi-mode interference among modified core modes and rod modes. This proposed sensor exhibits extremely high temperature and strain sensitivity and is compact in size because it is mounted by only a single element.

2. DEVICE FABRICATION

In the experiment, three adjacent air holes of an endlessly single-mode PCF (ESM-12, NKT Photonics) with hole diameter

of 3.6 μm and pitch of 7.9 μm were filled with an RI liquid (Cargille Labs, $n = 1.48$, at 25°C) by use of a femtosecond laser-assisted selective infiltration technique [18]. The filled RI liquid is capable of modifying the PCF core due to its higher RI compared with that of the background silica, and possesses a thermo-optic coefficient of -3.95×10^{-4} refractive index unit (RIU)/°C. The selective infiltration technique used here includes four steps: first, a section of PCF is spliced with a single-mode fiber (SMF) to block all the air holes in the cladding of the PCF; second, a section of ~10 μm long SMF away from the splicing point has been cut off and preserved by means of a precision cleaving device. As a result, all air holes in the cladding can be clearly observed through the thin SMF by use of an optical microscope; third, the three selected holes are drilled from the cross section of the SMF to the spliced facet by use of the focused femtosecond laser beam to make the selected holes open and enable the liquids to be selectively infiltrated into the PCF. Finally, one selectively opened end of the PCF is immersed into the RI liquid, and the non-immersed PCF end is left in the air in order to ensure that sufficient liquid is filled into the selectively opened PCF by capillary force after ~24 h. Figure 1(a) shows a schematic diagram of the setup in femtosecond laser-assisted selective infiltration. The pulse energy is continuously adjustable in the range between 0 and 4 mJ by rotating the half-wave plate (W) incorporated with a polarizer (P), and hence the on-target pulse energy can be precisely controlled. The PCF splicing with a section of SMF shown in the inset is achieved by precise cleaving. A cross section of the PCF after selective infiltration is shown in Fig. 1(b). The three adjacent bright spots in the innermost layer are rods filled with 1.48 RI liquids, and the white hexagon is the "liquid modified core". When the infiltration is completed, the modified PCF is spliced with SMF at both ends and its transmission spectrum is measured. To obtain a unique directional coupling loss dip and a proper interference fringe pattern, the PCF is cut back gradually from the non-immersed PCF end after each measurement to allow measurement of the transmission spectrum of the device with a different length, as shown in Fig. 2(a). The free spectral range (FSR) of the fringe pattern increases with the decrease of PCF length. The proposed device, with PCF length of ~0.91 cm, is obtained at the end. As shown in Fig. 2(b), besides the interference fringe pattern produced by the multimode interference, there is a unique transmission loss dip (Dip A) created by the directional coupling from the modified core mode to the rod mode. The strength of directional coupling resonance and interference are ~23.00 and ~5.00 dB,

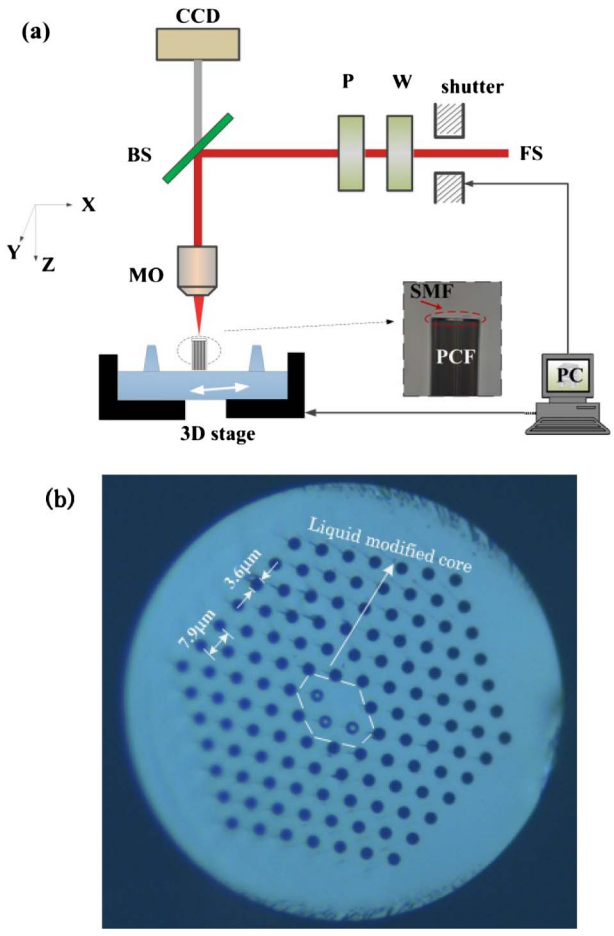

Fig. 1. (a) Schematic diagram of the femtosecond laser-assisted selective infiltration setup; inset, optical microscope image of a PCF with all holes sealed by a section of SMF. (b) Cross-sectional view of the PCF with three holes selectively infiltrated (white spot indicates the hole filled with standard 1.48-RI liquid).

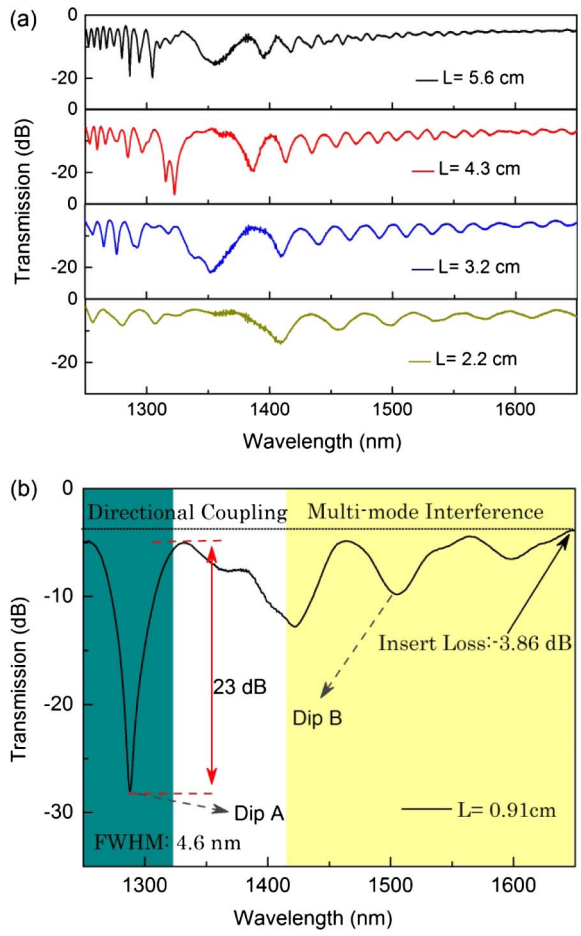

Fig. 2. (a) Transmission spectra of filled PCF with different length and (b) transmission spectrum of the proposed device.

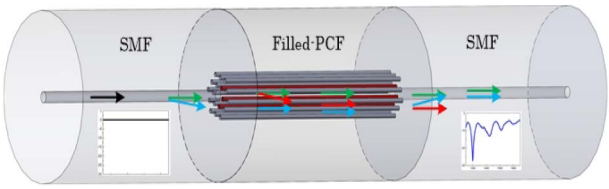

Fig. 3. Working principle of the proposed sensor. The liquid rods are highlighted in dark red.

respectively; the full width at half-maximum (FWHM) of dip A is ~4.6 nm and the insertion loss is ~3.86 dB. Unlike the PCF with one single filled hole in the second layer, which creates only one apparent transmission loss at the resonant wavelength [19], the PCF modified by three selectively infiltrated holes of the innermost layer will induce extra interference among the modified core modes and rod modes. The modal interference of the proposed sensor can be described by the equation

$$I = I_1 + I_2 + 2\sqrt{I_1 I_2}\cos\varphi, \tag{1}$$

where I_1 and I_2 are the light intensities of two modes involved in the interference, and φ is the phase of the interferometer. The FSR is given by

$$\mathrm{FSR} = \frac{\lambda^2}{\Delta n L}, \tag{2}$$

where λ is the wavelength, Δn is the effective RI difference between the two modes involved in the interference, and L is the length of the filled PCF. As shown in Fig. 3, the light is coupled from the amplified spontaneous emission source into a section of SMF and then propagates into the liquid modified PCF. A part of the light will go through the device in the modified core (green arrow) and another part of the light propagates into the rods (blue arrow), which will be coupled back to the SMF core at the next PCF–SMF splicing joint and interfere with the light propagating in the modified core (green arrow). Meanwhile, the light transmitting in the modified core will be coupled into the rods when the phase-matching condition is met (red arrow), which will emit into the cladding at the splicing joint and finally induce a dramatic loss of light intensity at the resonant wavelength. Finally, the light is coupled from the SMF into an optical spectrum analyzer (OSA, YOKOGAWA AQ6370C) for transmission spectrum measurement. The wavelength signals of these two different regimes have different responses to the same ambient temperature and applied strain so that they can be applied for dual-parameter measurement.

3. RESULTS AND DISCUSSION

Numerical simulations based on the finite element method are performed to quantitatively characterize the PCF with an embedded coupler and an interferometer. Here the simulation is modeled according to the measured data shown in Fig. 1(b), and the dispersions of fused silica are taken into account according to Sellmeier's formula [20]. The material dispersion of the liquid is fitted by the Cauchy equation [21] as follows:

$$n = a + \frac{b}{\lambda^2} + \frac{c}{\lambda^4}, \tag{3}$$

where λ is the operation wavelength. Constants a, b, and c are 1.4652×10^{-5}, 0.0051×10^{-5}, and 2.7139×10^{-5}, respectively. Although Cauchy's formula is precise only for the wavelength range from 400 to 700 nm, we can extrapolate them into the near-IR region with reasonable accuracy since the RI liquid used in the experiment exhibits low dispersion. The calculated profiles and dispersion curves of the guide modes are shown in Fig. 4(a). According to the coupled-mode theory, the mode coupling will occur when the effective RI of modes match to each other. The intersection region of the dispersion curves of modes (a) and (b) is ~1285 nm, which allows the light to be coupled from the modified core into the rods. Due to the large difference of material dispersion between liquid and solid, the dispersion curve of modes (a) and (b) will separate immediately after crossing, leading to the mismatching of effective RI of modes, which means that the mode coupling won't occur outside the intersection and results in a narrow mode-coupling region. This is different from the mode coupling between solid cores that occurs over a wide wavelength range, owing to the same or similar material dispersion. The profile of modes (a) and (b) in the intersection region can be also seen in Fig. 4(a), which is different from the mode profile outside the intersection region. In addition, there is no other cross of the mode-dispersion curve among the 10 guide modes in the wavelength region from 1250 to 1650 nm, so that there is no other mode-coupling region due to the effective RI mismatching of the

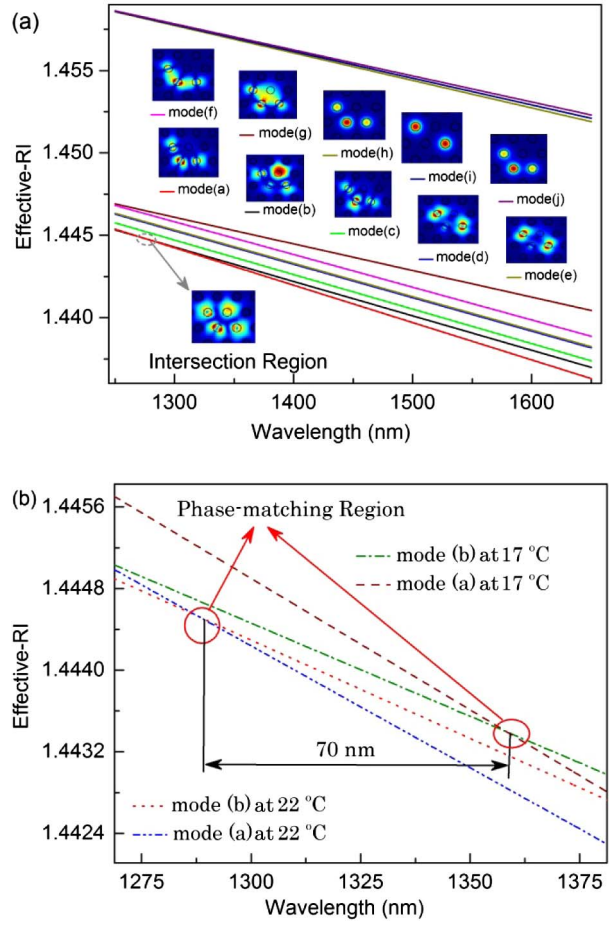

Fig. 4. (a) Calculated profiles and dispersion curves of the guided modes in the proposed device. (b) Phase-matching relationship of the coupling between the core and rod modes at 17°C and 22°C, respectively.

modes, which indicates that the mode-directional coupling will not have an effect on modal interference outside the narrow intersection region.

Because of the high thermo-optic coefficient of liquid, the effective RIs of modes (a) and (b) are very sensitive to the ambient temperature. In order to investigate the unique loss dip produced by mode-coupling response to temperature, the thermo-optic coefficients of liquid (-3.95×10^{-4} RIU/°C) and pure silica (8×10^{-6} RIU/°C) are taken into account. The dispersion of modes (a) and (b) at 17°C and 22°C are calculated and plotted in Fig. 4(b), and the blueshift of the intersection region is about 70 nm, which indicates that the calculated temperature sensitivity of the proposed device is up to −15 nm/°C.

At room temperature, a dramatic resonant loss dip and an interference fringe pattern based on different regimes can be measured expectably in the wavelength region from 1250 to 1650 nm, as shown in Fig. 3. The transmission spectra corresponding to the temperature range between 18°C and 21°C are demonstrated and plotted in Fig. 5(a). Dips A and B keep good profiles along with temperature variation all the time, and this proves that the crosstalk between the directional coupling and mode interference can be neglected. The measured dip wavelength is slightly different from the calculated one; this is because the real liquid RI values and the geometrical parameters

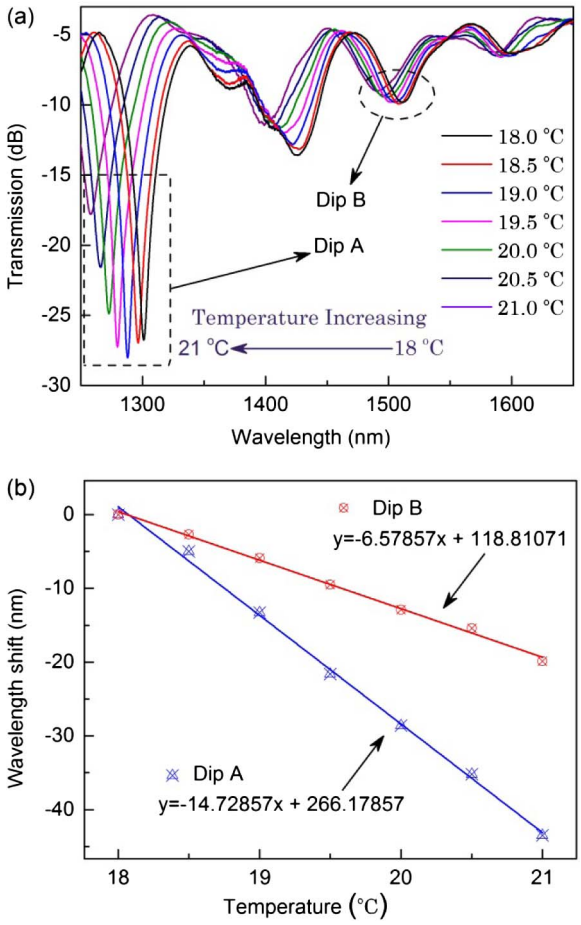

Fig. 5. (a) Transmission spectra evolution of the proposed device as temperature increases from 18°C to 21°C and (b) relationship between the temperature and wavelength shift of Dips A and B.

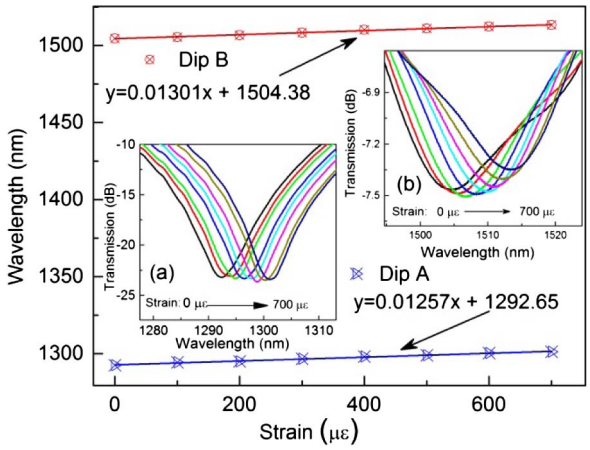

Fig. 6. Relationship between strain and shift of the wavelengths of the characteristic peaks. Insets (a) and (b) represent the variations of Dips A and B as the strain increases, respectively.

of the PCF cannot be fully consistent with the values used in the theoretical calculation. It can be noticed that the transmission spectrum shifts to the short wavelength as the temperature increases, which agrees well with the simulation result. Dip B, caused by the modal interference, shifts to the same direction as Dip A. Although the sensitivity of Dip B is lower than that of Dip A, it is much higher than the other dual-parameter sensors based on fiber tip modal interference [15] because of the high thermo-optic coefficient of the RI liquid. The sensitivity of Dips A and B are measured to be ~14.73 and ~6.58 nm/°C, respectively. Next we measured the strain response, with the strain varying from 0 to 700 με with an increment of 100 με. Figure 6 shows the wavelength shifts of the characteristic dips as the strain increases. Unlike the temperature response, both Dips A and B have a redshift as the strain increases. Their strain sensitivities are measured to be ~12.57 and ~13.01 pm/με, respectively. Therefore, after measuring the wavelength changes of the two dips, the temperature and strain variation ΔT and $\Delta\varepsilon$ can be simultaneously determined by solving the matrix equation

$$\begin{bmatrix} \Delta T \\ \Delta\varepsilon \end{bmatrix} = \begin{bmatrix} 14.73 & 6.58 \\ 12.57 & 13.01 \end{bmatrix}^{-1} \begin{bmatrix} \Delta\lambda_A \\ \Delta\lambda_B \end{bmatrix}. \quad (4)$$

4. CONCLUSION

A liquid modified PCF integrated with an embedded directional coupler and a multi-mode interferometer has been demonstrated. In this device, both multi-mode interference and the embedded coupler produced by mode coupling between the modified core and rod modes are investigated in experiment and simulation. The wavelength signals of these two different regimes have different responses to the same ambient temperature and applied strain so that they can be applied for simultaneous temperature and strain measurement. The measured temperature sensitivity is up to ~14.73 nm/°C, which shows a good agreement with the calculated temperature sensitivity, and the strain sensitivity is measured to be ~13.01 pm/με.

This device is promising for applications in high-sensitivity dual-parameter sensors.

†These authors contributed equally to this work.

Funding. National Natural Science Foundation of China (NSFC) (61635007, 61425007, 61377090, 61575128); Guangdong Science and Technology Department (2014A030308007, 2014B050504010, 2015B010105007, 2015A030313541); Science and Technology Innovation Commission of Shenzhen (GJHZ20150313093755757, JCYJ20160520163134575, JCYJ20160427104925452); Pearl River Scholar Fellowships.

REFERENCES

1. D. K. C. Wu, B. T. Kuhlmey, and B. J. Eggleton, "Ultrasensitive photonic crystal fiber refractive index sensor," Opt. Lett. **34**, 322–324 (2009).
2. M. Luo, Y. G. Liu, Z. Wang, T. Han, Z. Wu, J. Guo, and W. Huang, "Twin-resonance-coupling and high sensitivity sensing characteristics of a selectively fluid-filled microstructured optical fiber," Opt. Express **21**, 30911–30917 (2013).
3. Y. Wang, C. R. Liao, and D. N. Wang, "Embedded coupler based on selectively infiltrated photonic crystal fiber for strain measurement," Opt. Lett. **37**, 4747–4749 (2012).
4. K. J. Lee, X. Liu, N. Vuillemin, R. Lwin, S. G. Leon-Saval, A. Argyros, and B. T. Kuhlmey, "Refractive index sensor based on a polymer fiber directional coupler for low index sensing," Opt. Express **22**, 17497–17507 (2014).
5. Z. Xu, J. Lim, D. J. Hu, Q. Sun, R. Y. Wong, K. Li, M. Jiang, and P. P. Shum, "Investigation of temperature sensing characteristics in selectively infiltrated photonic crystal fiber," Opt. Express **24**, 1699–1707 (2016).
6. B. Sun, Z. Zhang, W. Wei, C. Wang, C. Liao, L. Zhang, and Y. Wang, "Unique temperature dependence of selectively liquid-crystal-filled photonic crystal fibers," IEEE Photon. Technol. Lett. **28**, 1282–1285 (2016).
7. J. Guo, Y.-G. Liu, Z. Wang, T. Han, W. Huang, and M. Luo, "Tunable fiber polarizing filter based on a single-hole-infiltrated polarization maintaining photonic crystal fiber," Opt. Express **22**, 7607–7616 (2014).
8. H. F. Chen, Y. Wang, and D. N. Wang, "Selectively infiltrated PCF for directional bend sensing with large bending range," IEEE Photon. Technol. Lett. **27**, 502–505 (2015).
9. M. Yang, D. N. Wang, Y. Wang, and C. R. Liao, "Fiber in-line Mach–Zehnder interferometer constructed by selective infiltration of two air holes in photonic crystal fiber," Opt. Lett. **36**, 636–638 (2011).
10. H. Z. Yang, X. G. Qiao, Y. P. Wang, M. M. Ali, M. H. Lai, K. S. Lim, and H. Ahmad, "In-fiber gratings for simultaneous monitoring temperature and strain in ultrahigh temperature," IEEE Photon. Technol. Lett. **27**, 58–61 (2015).
11. H. Liu, H. Z. Yang, X. Qiao, M. Hu, Z. Feng, R. Wang, Q. Rong, D. S. Gunawardena, K.-S. Lim, and H. Ahmad, "Strain measurement at high temperature environment based on Fabry–Perot interferometer cascaded fiber regeneration grating," Sens. Actuators A **248**, 199–205 (2016).
12. Y.-J. Rao, Z.-l. Ran, X. Liao, and H.-Y. Deng, "Hybrid LPFG/MEFPI sensor for simultaneous measurement of high-temperature and strain," Opt. Express **15**, 14936–14941 (2007).
13. Q. Liu, Z. L. Ran, Y. J. Rao, S. C. Luo, H. Q. Yang, and Y. Huang, "Highly integrated FP/FBG sensor for simultaneous measurement of high temperature and strain," IEEE Photon. Technol. Lett. **26**, 1715–1717 (2014).
14. Y. Jiang, D. Yang, Y. Yuan, J. Xu, D. Li, and J. Zhao, "Strain and high-temperature discrimination using a type II fiber Bragg grating and a miniature fiber Fabry–Perot interferometer," Appl. Opt. **55**, 6341–6345 (2016).
15. C. Chen, Y. S. Yu, X. Y. Zhang, R. Yang, C. C. Zhu, C. Wang, Y. Xue, F. Zhu, Q. D. Chen, and H. B. Sun, "Compact fiber tip modal interferometer for high-temperature and transverse load measurements," Opt. Lett. **38**, 3202–3204 (2013).
16. S. Rota-Rodrigo, M. Lopez-Amo, J. Kobelke, K. Schuster, J. L. Santos, and O. Frazao, "Multimodal interferometer based on a suspended core fiber for simultaneous measurement of physical parameters," J. Lightwave Technol. **33**, 2468–2473 (2015).
17. H. F. Chen, D. N. Wang, and Y. Wang, "Simultaneous strain and temperature sensing using a slightly tapered optical fiber with an inner cavity," Analyst **140**, 1859–1862 (2015).
18. Y. Wang, C. R. Liao, and D. N. Wang, "Femtosecond laser-assisted selective infiltration of microstructured optical fibers," Opt. Express **18**, 18056–18060 (2010).
19. Y. Wang, M. Yang, D. N. Wang, and C. R. Liao, "Selectively infiltrated photonic crystal fiber with ultrahigh temperature sensitivity," IEEE Photon. Technol. Lett. **23**, 1520–1522 (2011).
20. I. H. Malitson, "Interspecimen comparison of the refractive index of fused silica," J. Opt. Soc. Am. **55**, 1205–1209 (1965).
21. P. R. Cooper, "Refractive-index measurements of liquids used in conjunction with optical fibers," Appl. Opt. **22**, 3070–3072 (1983).